ARTICLE

# Pattern Placement Accuracy in Block Copolymer Directed Self-Assembly Based on Chemical Epitaxy

**Gregory S. Doerk,* Chi-Chun Liu,‡ Joy Y. Cheng, Charles T. Rettner, Jed W. Pitera, Leslie E. Krupp, Teya Topuria, Noel Arellano, and Daniel P. Sanders**

IBM Almaden Research Center, 650 Harry Road, San Jose, California 95120, United States

**ABSTRACT** The realization of viable designs for circuit patterns using the dense features formed by block copolymer directed self-assembly (DSA) will require a precise and quantitative understanding of self-assembled feature registration to guiding templates or chemical prepatterns. Here we report measurements of DSA placement error for lamellar block copolymer domains indexed to specific lines in the surface chemical prepattern for spatial frequency tripling and quadrupling. These measurements are made possible by the use of an inorganic domain-selective prepattern material that may be imaged upon polymer removal after DSA and a prepattern design incorporating a single feature serving as an *in situ* registration mark that is identifiable by pattern symmetry in both the prepattern and resulting self-assembled pattern. The results indicate that DSA placement error is correlated with average prepattern line width as well as prepattern pitch uniformity. Finally, the magnitude of DSA placement error anticipated for a uniform, optimized prepattern is estimated.

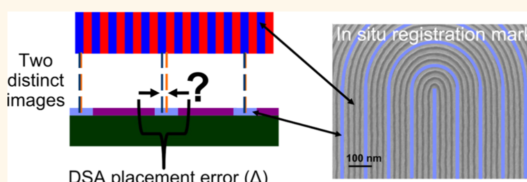


**KEYWORDS:** directed self-assembly · chemical epitaxy · block copolymer · placement error · lithography

Pattern feature downscaling to reduce cost per device is a primary driver for the success of microelectronics and related industries, but the practical resolution limit at ~40 nm half-pitch for 193 nm water immersion (193i) photolithography[1] and the lack of immediately available next-generation lithography alternatives such as parallel electron-beam lithography or extreme ultraviolet lithography have generated significant interest in extensions to current 193i-based patterning for sublithographic resolution. In particular, directed self-assembly (DSA) of diblock copolymers has become a distinct candidate to multiply the spatial density of lithographically defined features. Guiding of DSA-defined features is achieved through the use of lithographically defined topographical templates (graphoepitaxy[2−8]) or chemical prepatterns on the underlying substrate (chemical epitaxy[7,9−13]). Both methods can enhance resolution by multiplying the spatial frequency of the lithographic prepattern, but defects and nonuniformity in chemical prepatterns are substantially rectified with the use of chemical epitaxy. Strong adherence to feature dimensions set by the size of the block lengths preserves uniformity in the DSA pattern away from the interface with the chemical prepattern, leading to improved critical dimension (CD) and pattern placement uniformity,[11,12] healing of minor prepattern defects,[12] and reduction of line-edge roughness.[12,14]

Recent demonstrations of compatible integration of DSA based on chemical epitaxy with 193i lithography materials and processes across full 300 mm wafers[7,15−17] have enabled assessments of defectivity, line-edge roughness, pattern uniformity, and pattern transferability at a scale necessary for high-volume manufacturing, bringing DSA a step closer to potential adoption by the semiconductor industry. One of the most immediate prospects for patterning processes based on chemical epitaxy is the patterning of dense line-space arrays,[7,12] which may be used for bit-patterned media[18] or for gridded unidirectional circuit layouts. However, in patterning applications where complex patterns on multiple layers must be precisely aligned with each other, overlay and pattern

* Address correspondence to gsdoerk@us.ibm.com.

Received for review August 29, 2012 and accepted November 30, 2012.

Published online November 30, 2012
10.1021/nn303974j

© 2012 American Chemical Society

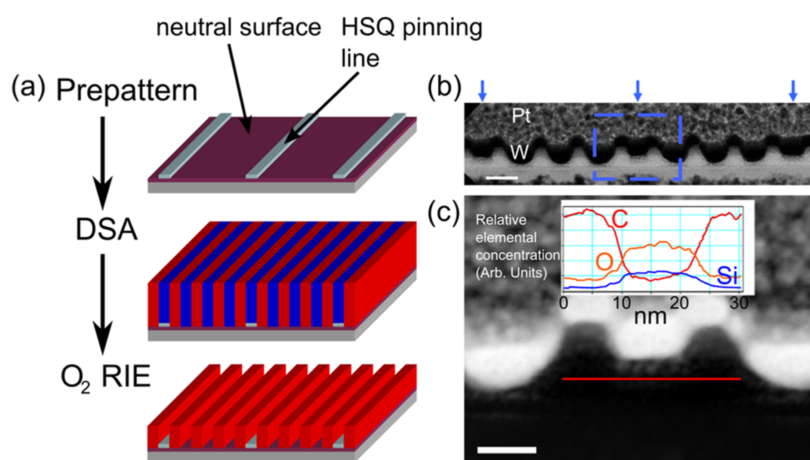


**Figure 1. (a) Schematic of the DSA process flow using PS-PMMA. A chemical prepattern is composed of thin HSQ lines on a cross-linked neutral surface that orients PS and PMMA blocks perpendicularly to the substrate. After casting PS-PMMA and thermally annealing the PMMA domains register with the HSQ lines by selective chemical affinity. An oxygen RIE is used to preferentially remove PMMA domains. (b) Cross-sectional bright-field TEM image of an as-etched DSA-generated line-space array. Blue arrows mark the positions of shallow trenches directly above HSQ pinning lines (scale bar = 20 nm). (c) Higher magnification Z-contrast STEM image of a single pinning line in the area marked by a dashed box in (b) (scale bar = 10 nm). An EELS line scan was taken along the length demarcated by a red line, and the results are included in the inset graph. The presence of HSQ is confirmed by a higher silicon and oxygen content under the shallow trench.**

placement error are major contributions to the total error tolerance.

This demands a detailed understanding of placement accuracy for DSA processes. Previous efforts to characterize DSA pattern placement have used fitting of the spatial locations of domain centroids in registration with a particular lattice model. For example, Liu *et al.* fitted horizontal lines (by a least-squares fit) of centroids of DSA-generated holes that were hexagonally positioned to obtain a better definition of the reciprocal lattice vector and in turn generating more accurate translational order parameters.[19] Ruiz *et al.*, on the other hand, used a least-squares fit of rectangular features generated partially through DSA to a rectangular lattice and used the standard deviation in residual vector displacements between the measured centroid positions and the best fit lattice points to quantify placement accuracy.[18] In essence, by considering registration to ideal lattices, both measurements provide an estimation of post-DSA uniformity. However, where overlay registration marks for subsequent patterning steps after DSA will be placed at or beneath the chemical prepattern layer, placement accuracy of DSA features must also be measured in reference to registration with the underlying prepattern. Contrast variations between domains in images of the block copolymer after DSA may reveal what domains lie above different features in the chemical prepattern,[13] but the prepattern itself is not evident in these images; accurate and quantitative position extraction from both the prepattern and the DSA pattern are therefore not possible using the same image, rendering the measurement of placement accuracy for DSA features in reference to features in the underlying prepattern particularly difficult for chemical epitaxy processes.

Herein we present measurements of block copolymer DSA placement accuracy in registration of the guiding prepatterns for chemical epitaxy processes. Our focus is on the DSA of a symmetric polystyrene-block-poly(methyl methacrylate) (PS-PMMA) diblock copolymer that forms lamellae with a 25 nm pitch, although the strategy based on *in situ* registration marks employed here will be applicable to the chemical epitaxy DSA of block copolymers with different constituent blocks, domain sizes, or morphologies. We first discuss the advantages of using chemical prepatterns with *in situ* registration marks having a unique center defined by pattern symmetry and composed partially of an inorganic material selectively wetted by one block. We then analyze the effects of the prepattern line CD values and the nonuniformity of the prepattern on DSA placement error. A negative correlation between average prepattern line CD and DSA placement error is found, and comparison with root-mean-squared DSA placement error calculations based upon a simple one-dimensional free-energy model for lamellar chemoepitaxy implies that a minimum DSA placement error may be achieved for prepattern line CD values at or slightly above half the natural period of the lamellar block copolymer. On the other hand, a stronger correlation between DSA placement error and prepattern placement error is identified as a consequence of the capability for block copolymers used in chemoepitaxial DSA to rectify defects and nonuniformities in the chemical prepattern.

## RESULTS AND DISCUSSION

The basic process flow for chemical epitaxy of PS-PMMA lamellae used in this work is depicted schematically in Figure 1a, following the methods described in

previous work.[12] The chemical pattern is composed of hydrogen silsesquioxane (HSQ) lines 2−5 nm in height on top of a cross-linked underlayer that presents a neutral surface orienting PS-PMMA lamellae perpendicularly to the substrate. Through selective wetting, the HSQ lines serve to pin the PMMA domains during DSA. The pinning line pitches are nominally 75 or 100 nm to achieve frequency tripling (3×) or quadrupling (4×) for the lamellae that have an approximately 25 nm natural period ($L_o$). DSA is performed by casting films with thicknesses ($t$) of either ∼37 or ∼48 nm onto the chemical prepattern and thermally annealing. To obtain sufficient image contrast, an oxygen reactive ion etch (RIE) is used to preferentially remove the PMMA domains; the former PMMA domains are replaced by spaces in the resultant line-space pattern after etch.

A key reason that measuring placement accuracy in reference to the chemical prepattern for chemical epitaxy DSA has not been performed previously is that upon casting the block copolymer, the chemical prepattern can no longer be seen, in contrast to graphoepitaxy, where the block copolymer pattern and the topographical template are often coincident in the same image. Therefore, chemical prepatterns must be imaged before or after DSA. The surface chemistry of the prepattern is a critical feature to successful DSA but may also be highly sensitive to changes induced by the imaging process, as for example by the energy added from an electron beam. Due to these changes to the prepattern surface chemistry, prior imaging may affect or even obstruct DSA. However, since the materials making up the chemical prepatterns are typically organic, they are often removed along with the block copolymer during the plasma etch. Organic prepatterns also provide negligible Z-contrast differences within the prepatterns and between the prepatterns and most block copolymers in images obtained through electron microscopy, as all the materials of interest are primarily composed of carbon. These aspects make it extremely difficult to image a block copolymer pattern and its corresponding chemical prepattern in the exact same location under normal conditions. As an inorganic pinning material on the other hand, HSQ is resistant to the oxygen RIE, so that continued polymer removal by RIE after imaging the DSA pattern may be used to recover the HSQ chemical prepattern for imaging after DSA.

The etch resistance and silicon content of HSQ enable direct visualization of DSA-prepattern registration for chemical epitaxy in cross-section transmission electron microscope (TEM) images after PMMA removal, as shown for example in the bright-field TEM image of a line-space array provided in Figure 1b. Tungsten and platinum are present above the line-space array, as they were necessary to preserve the block copolymer morphology during cross-sectioning. Trenches left by PMMA removal are noticeably shallower over pinning lines given that HSQ acts as an etch stop for the oxygen RIE. These pinned trenches are marked by blue arrows. To confirm and measure the position of HSQ lines under these shallow trenches, we examined higher magnification Z-contrast scanning transmission electron microscope (STEM) images of individual pinning lines (*i.e.*, shallow trenches) such as in Figure 1c. Analysis of the one-dimensional spatial distribution of relative atomic concentration across the expected location of HSQ was performed using electron energy loss spectroscopy (EELS). The results of an EELS line scan marked in red in Figure 1c are shown in the inset to that figure, indicating the presence of HSQ by the increased relative concentration of silicon and oxygen and the reduced concentration of carbon.

While TEM imaging is useful as a direct visualization of PMMA pinning by HSQ, the time required for sample preparation seriouly limits the volume of data that can be collected. Plan view imaging of prepatterns and resulting DSA patterns would be more amenable to collection of large volumes of data and subsequent statistical analyses, but as noted previously the precise position of pinning lines under the resulting DSA patterns are largely indeterminable. It is thus necessary to identify at least one pinning line and the exact block copolymer domain(s) that it pins. Registration marks in or beneath the prepattern layer may be used to measure relative alignment between the prepattern and block copolymer, but they are not typically visible under the block copolymer layer using the imaging techniques with adequate resolution to measure block copolymer domain positions (i.e., atomic force microscopy or electron microscopy). Larger non-line-pinning features in the prepattern that force lamellae directly above to assume an orientation parallel to the substrate may serve as registration marks for both the prepattern and the block copolymer pattern. However, nonabrupt transitions in lamellar orientation at the registration mark edges preclude precise identification of its true centroid in images of the block copolymer layer. Furthermore, these larger features that guide lamellae into a substrate-parallel orientation require the existence of a grain boundary, or even a discontinuity in lamellae,[20] that tends to increase the prevalence of defects in the imaging area.

Greater success is to be expected with prepattern designs that identify at least one pinning line and its corresponding pinned line or space while preserving the continuity of most lamellae to minimize the likelihood for defect formation. We achieve this by attaching concentric semicircular pinning lines to the end of an array of straight pinning lines such that the straight pinning lines run continuously into the semicircle pinning lines, with one single pinning line at the center, as depicted schematically in Figure 2a. By using a prepattern with a unique central feature that results in a single self-assembled domain at the center of the

DSA-generated pattern clearly identifiable by pattern symmetry, we generate a type of registration mark *in situ* during DSA that is shown schematically in Figure 2b. In the case of HSQ with PS-PMMA, the center feature is a space. This central space is linked with the central pinning line, and each pinning line of index $j$ from the central pinning line may be linked with each space of index $f$ multiplied by $j$ from the central space in the self-assembled pattern, where $f$ is the frequency multiplication factor (3 or 4).

Figure 3 provides an example of the process used to obtain DSA placement error values for a single prepattern. In this work, pattern placement error is extracted from a scanning electron microscope (SEM) image of the prepattern and a SEM image of the DSA pattern. However, since the SEM images are taken at distinct times, the central pinning lines and central DSA spaces will possess centroid locations at different distances from the left edge of their respective images, inducing a constant $x$-offset between the position of the $j$th pinning line and the corresponding DSA space. We etched each self-assembled pattern (Figure 3a) using an oxygen RIE to an intermediate stage where pinning lines and some remaining PS lines are present in the same image, shown in Figure 3b. After this, we further etched the sample to remove the polymer completely, revealing the recovered prepatterns for imaging as shown in Figure 3c. Both the self-assembled pattern image and the prepattern image are registered to the intermediate image using the MATLAB multimodal image registration function, effectively removing the $x$-offset between the images. The registered images are both thresholded, resulting in binary images of the DSA pattern and the prepattern such as Figure 3d and e, respectively, so that DSA space and pinning line centroids may be obtained. The DSA placement error $\Delta_j$ for the $j$th pinning line is then defined by

$$\Delta_j = X_{f\times j,\,\mathrm{DSA}} - X_{j,\,\mathrm{prepattern}} \tag{1}$$

where $X_j$ is the centroid $x$-coordinate for the $j$th pinning line with respect to the central pinning line. Note that both the central pinning line and the central DSA space are assigned an index of zero.

The results of analysis of the DSA pattern placement error are summarized in Table 1. Four data categories are included, based on frequency tripling ($f$ = 3) or quadrupling ($f$ = 4) for 37 or 48 nm thick block copolymer films, and averages are taken over the number of image sets in each category. The magnitude of the mean DSA placement error is less than 0.4 nm across the categories, though it is generally less than 3 times the standard error, indicating that it is potentially zero statistically. The placement error 3$\sigma$ values

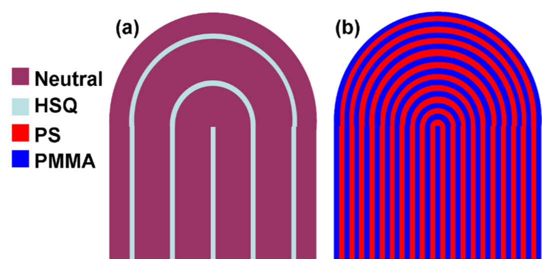


**Figure 2. Schematic illustration of the *in situ* registration mark specifically employed in this work. (a) Chemical prepattern design used for DSA placement accuracy measurements. (b) Resulting self-assembled pattern with a central PMMA domain identifiable by pattern symmetry.**

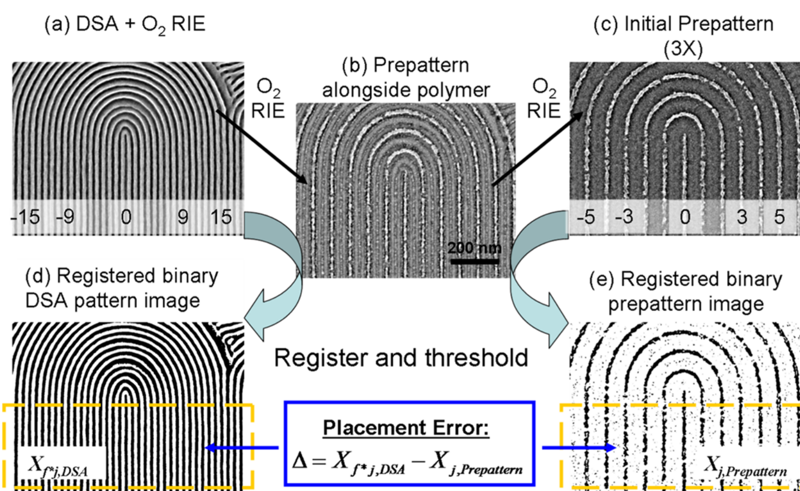


**Figure 3. Example of DSA placement error measurement for a single prepattern designed for DSA spatial frequency tripling. All SEM images have been filtered with contrast enhancement, and all images are at the same magnification. (a) SEM image of the DSA pattern after initial $O_2$ RIE treatment. (b) SEM image of the same pattern after further $O_2$ RIE treatment that shows both HSQ prepattern lines and remaining though diminished PS lines. (c) SEM image after a third $O_2$ RIE treatment to recover the HSQ prepattern. Images (d) and (e) are binarized versions of images (a) and (c), respectively, after co-registration with image (b). Centroid measurements are limited to regions with vertical lines only by limiting analyses to the area delineated by the gold dashed bounding rectangle. The numbers shown in (a) and (c) are indices in reference to the central image feature for DSA spaces and pinning lines, respectively.**

(herein reported in accordance with standard practices of the microelectronics industry), where $\sigma$ is the standard deviation, are in the range ~2–3 nm. In order to minimize pattern placement error in high-volume manufacturing using DSA though, it is critical to understand the contributions of chemical prepattern characteristics to the DSA placement error, and the relative importance of nanometer-scale local uniformity and geometry of the chemical prepattern for DSA placement error (rather than global alignment factors that affect standard photolithography).

Chemoepitaxial DSA with density multiplication is acknowledged to display high sensitivity in the quality and defectivity of the self-assembled pattern on prepattern chemistry and geometry,[21] with optimum behavior expected for line-space patterns derived from equal block volume lamellae-forming diblock copolymers using prepatterns having pinning line critical dimensions in the vicinity of $0.5L_o$.[12,13] Therefore, it is of interest to study the impact of average pinning line CD on the pattern placement error for block copolymer lamellae features. Figure 4a shows a plot of DSA placement error ($3\sigma$) as a function of average prepattern line CD in which it is evident that the placement error is negatively correlated with prepattern line CD (Pearson's $r = -0.5$) within the range of available data. Each data point represents a single prepattern.

**TABLE 1. Summary of DSA Placement Error Measurement Results**

| | | average DSA placement error (nm) | |
|---|---|---|---|
| *f* | *t* (nm) | mean[a] | $3\sigma$ |
| 3 | 37 | 0.4 ± 0.3 | 2.3 |
| 4 | 37 | 0.3 ± 0.4 | 3.1 |
| 3 | 48 | 0.1 ± 0.3 | 3.2 |
| 4 | 48 | −0.2 ± 0.4 | 2.7 |

[a] Stated uncertainty is 3 times the standard error of the mean.

To help explain the observed trend, we calculated the system free energy as a function of $\Delta$ using a simple one-dimensional model for a single pinning line flanked by two other pinning lines, as depicted in Figure 4b. This geometry represents DSA spatial frequency quadrupling. The film thickness used in the model was ~37 nm, nearly identical with the thinner PS-PMMA films investigated experimentally. The pinning line width, $w$, was varied as a parameter in each calculation. We also considered two descriptions of the lamellar domain shape in the substrate normal direction. In the first, or "vertical", case, the interface between block copolymer domains is constrained to lie along the substrate normal, whereas in the second, or "tilt", case this interface is allowed to tilt in order to accommodate more or less interfacial area for the pinned domains at pinning line surfaces (see Experimental Section for details about the calculations using

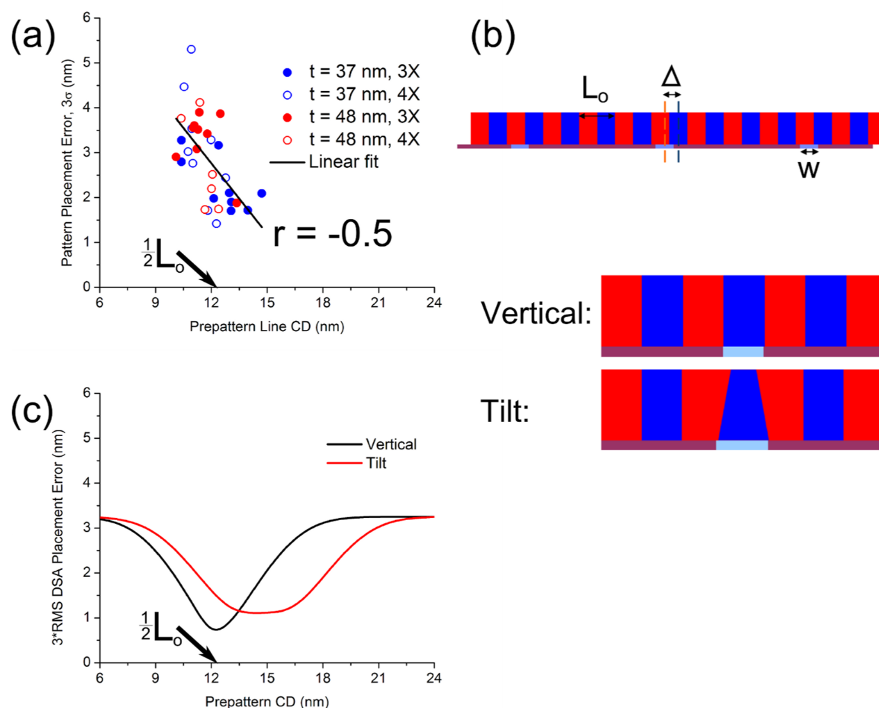


**Figure 4. Effect of pinning line CD (width) on DSA placement error. (a) Plot of DSA placement error ($3\sigma$) *vs* average pinning line CD. Each data point corresponds to a single prepattern. (b) Schematic of the geometry used in the DSA placement error calculation described in the text, including the "vertical" and "tilt" descriptions of the PS domain interfaces for pinned PMMA domains. This geometry represents spatial frequency quadrupling.(c) Calculated 3 × rms DSA placement error as a function of the pinning line width, *w*, for vertical and tilt cases of spatial frequency quadrupling. The arrows in (a) and (c) indicate $w = 0.5L_o$.**

this model for both cases). Consideration of the tilt case is important, as deformation of single lamellae domains by the epitaxy process is supported by both simulations[22] and experiment.[23] The preferential wetting of the HSQ pinning line by PMMA rather than PS leads to lower system free energies when the HSQ is entirely wetted by PMMA alone. For a prepattern pitch commensurate with a multiple of $L_o$, the expected value of $\Delta$ at equilibrium is zero. This is analogous with the mean DSA placement error. The root mean squared (rms) $\Delta$, on the other hand, is comparable to the experimentally measured $\sigma$; trends in experimental $3\sigma$ data are likely to be reflected in the calculated 3(rms) DSA placement error. From each free energy calculation at 1 nm increments in $w$ we extracted the rms DSA placement error (details are provided in the Experimental Section) as a function of $w$, the results of which are plotted in Figure 4c. Calculations for vertical as well as tilt cases are both provided, as the amount of deformation experienced by PMMA domains above HSQ pinning lines is unknown experimentally.

For $w \approx 0.5L_o$, or the width of one PMMA domain, the system free energy increases proportionally to the absolute value of $\Delta$ from a minimum value at $\Delta = 0$. This is because any value of $\Delta$ at this pinning line width increases the PS-HSQ interfacial area (vertical case) or causes the pinned PMMA domain to deform (tilt case), increasing the system free energy. The rms $\Delta$ is near its lowest values due to this high energetic penalty. When $w < 0.5L_o$, the system free energy is approximately equivalent for multiple values of $\Delta$ if the pinning line lies entirely underneath a PMMA domain only, pushing up the rms $\Delta$. On the other side, for $w > 0.5L_o$ system free energy increases for the vertical case as PS is forced to wet the pinning line, though again the system free energy will be approximately the same for multiple $\Delta$ values at fixed $w$, increasing the rms $\Delta$. However, with tilt deformation the system is stabilized at its lowest free energy across a range of $w$ values since the energetic penalties arising from polymer chain stretching and increasing PS-PMMA interfacial area are offset by the reduced penalty due to increased PS-HSQ interfacial area. Within this range of $w$, PS-PMMA interfacial area and its associated energy penalty increase with the magnitude of $\Delta$, but this is negligibly impacted by the exact value of the pinning line width. Therefore, the rms DSA placement error is almost constant in the range of $w$ where the system free energy is stable. In total, the model predicts a minimum in the rms value of $\Delta$ at $w \approx 0.5L_o$ (~12.5 nm) for the vertical case and a slightly higher minimum rms registration error that is flat in the range 13−16 nm for the tilt case.

There is qualitative agreement between the model generally for pinning line CDs at or below the predicted range for minimum DSA placement error. Unfortunately, defect-free self-assembly was not obtained in the semicircular sections of the prepattern/DSA pattern for pinning line CDs larger than ~15 nm, prohibiting comparison of experimental DSA placement error values with the model for larger pinning line CDs. Nevertheless, the available data indicate that DSA placement error is negatively correlated with mean pinning line CD below ~$0.5L_o$ and that a minimum DSA placement error can be obtained using pinning lines with CDs equal to or slightly above $0.5L_o$, conveniently coincident with values predicted for minimum DSA pattern defectivity. The implicit scaling of the model calculations by $L_o$ suggests that this relationship between prepattern dimensions and DSA placement error should extend to other block copolymer lamellae systems with different natural periods. Since the model does not impose unique physical characteristics to the HSQ pinning lines beyond the PS-HSQ surface tension, we expect the trends observed in the model will be applicable to generic pinning materials such as dense or cross-linked polymers. However, the model does not treat cases where the pinning material may interpenetrate the overlying block copolymer, as may be possible for polymer brushes. More sophisticated models may be necessary to describe DSA placement accuracy in these systems.

Despite the qualitative agreement found in Figure 4, it is clear that experimentally measured DSA placement errors are systematically larger than those predicted by the model. However, the model presented here represents an ideal case not available in this system where prepatterns exhibit multiple types of variation (CD uniformity, CD line-edge roughness or line width roughness, and prepattern line placement error). The balance of strain and interfacial energies in a block copolymer results in narrowly defined dimensions and pitches with greater uniformity than is often possible in the prepatterns used to guide them, giving rise to the pattern rectification property that has been witnessed for chemical epitaxy DSA with density multiplication, but the implications of this property for the DSA placement accuracy as defined here are not yet known. Consider for instance a chemical prepattern with a nominal pitch that is commensurate with a multiple of $L_o$ but in which the measured pinning line centroids vary stochastically about their nominal positions designated using a linear least-squares best fit. Prepattern placement error is defined as the difference between the measured prepattern line centroids and their nominal values, provided directly by the residual values of the fit.[18] For defect-free self-assembled line-space patterns aligned along the total prepattern direction but with superior dimensional uniformity, we anticipate the pinned domain centroids to fall more closely upon the nominal pinning line centroid positions. Since the DSA placement error as defined here is the difference between the measured DSA centroids and the measured prepattern line centroids, then

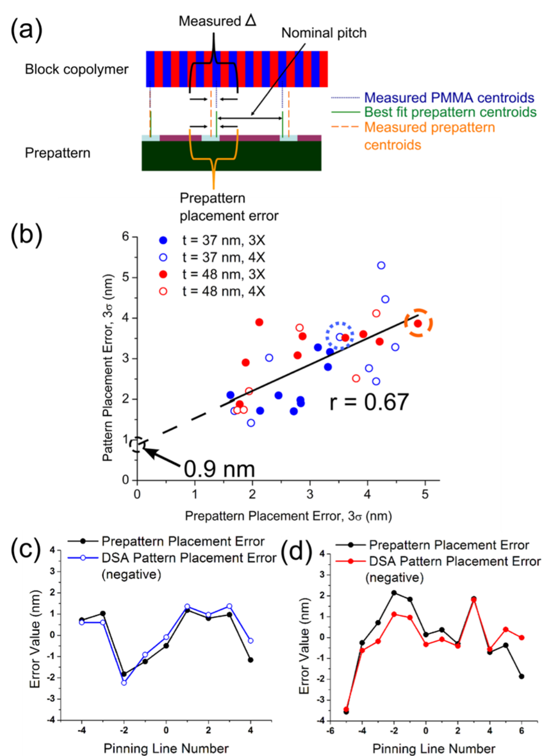


**Figure 5. Effect of prepattern pitch variation on DSA placement error. (a) Schematic depiction of the proposed relationship between prepattern placement error and DSA placement error. (b) Plot of DSA placement error ($3\sigma$) *vs* prepattern placement error ($3\sigma$). Each data point corresponds to a single prepattern. (c and d) Prepattern placement error values and corresponding DSA placement error values for the same pinning lines for prepatterns representing frequency quadrupling and tripling ((c) and (d), respectively).**

according to this argument, the DSA placement error will be approximately equal in magnitude but opposite in sign to the prepattern fit residuals as a direct consequence of the self-healing behavior inherent in DSA, illustrated schematically in Figure 5a. Though block copolymer domain deformation in close proximity to the pinning line interface may render this description not completely accurate,[22,23] it is likely to be a fair description further away from the pinning line interface and is more closely represented by the data obtained *via* plan view imaging.

Acknowledging the possibility of other contributions to measured DSA placement error values, this hypothesis predicts generally a positive correlation between the $3\sigma$ prepattern placement error and the $3\sigma$ DSA placement error. This positive correlation is indeed demonstrated in the plot of DSA placement error *versus* prepattern placement error shown in Figure 5b (Pearson's $r = 0.67$). Further corroboration of this hypothesis is obtained from examining the prepattern placement error and negative DSA placement error values ($-\Delta$) in individual image sets. Plots of these two measured parameters against the indexed number of their pinning line, as for example in

**TABLE 2. Summary of Unpinned DSA Placement Error Measurement Results**

| | | average DSA placement error (nm) | | | |
|---|---|---|---|---|---|
| $f$ | $t$ (nm) | unpinned mean | unpinned $3\sigma$ | pinned $3\sigma$ | pinned/unpinned $3\sigma$ correlation coefficient |
| 3 | 37 | 0.3 | 1.7 | 2.3 | 0.52 |
| 4 | 37 | 0.3 | 2.0 | 3.1 | 0.83 |
| 3 | 48 | 0.1 | 2.2 | 3.2 | 0.66 |
| 4 | 48 | −0.1 | 1.9 | 2.7 | 0.71 |

Figure 5c and d, which correspond to the circled data points in Figure 5b (a blue-dotted circle and red-dashed circle, respectively), show that the $-\Delta$ values tend to track the prepattern placement error values reasonably well.

Much of the variation in the prepatterns found in this work arises due to the experimental techniques used to generate them, and this variation may be reduced with improved process control; for instance, we have found the typical $3\sigma$ pitch variation in 100 nm pitch gratings created using 193i lithography is less than 1 nm. Therefore, it is of interest to estimate the likely magnitude of DSA placement errors for perfectly uniform prepatterns. We obtain this estimate from the intercept in the linear least-squares fit to the data plotted in Figure 5b. On this basis, the DSA placement error $3\sigma$ in the limit of an optimized prepattern should approach 0.9 nm, with a value less than 2.2 nm with 99.7% confidence. Even a more conservative estimate for optimized DSA placement error values of approximately $\sim$1−2 nm is still significantly less than the overlay error of $\sim$5 nm expected from patterning with photolithography scanners.[24,25]

Up to this point, we have addressed only DSA placement error for pinned PMMA domains, but the DSA features not lying directly upon pinning lines are equally important with regard to envisioned patterning applications. For proper comparison with the DSA placement error for pinned domains, we define an unpinned DSA placement error by interpolation between pinning line centroids measured in the prepattern images. If $k$ is taken to be a positive-valued index of DSA spaces between pinning lines with values from 1 to $(f-1)$, then the pattern placement error $\Delta_k$ for the $k$th space (between $j$ and $j \pm 1$ pinning lines) may be defined as

$$\Delta_k = X_{f \times j \pm k, \mathrm{DSA}} - \left[\frac{f-k}{f}X_j + \frac{k}{f}X_{j \pm 1}\right]_{\mathrm{prepattern}} \quad (2)$$

where the $\pm$ in subscripts is addition (subtraction) on the right (left) side of the central pinning line. The results of these unpinned DSA placement error measurements are summarized in Table 2. Cursory examination of the unpinned DSA placement $3\sigma$ values reveals that they are less than the respective pinned

DSA placement error 3$\sigma$ values. Given the high pitch uniformity for the block copolymer, the unpinned placement error between two pinning lines may be thought of as averaging between the DSA placement error for the two exterior pinning lines, but over more data points. Therefore the unpinned placement error will be less than and positively correlated with the pinned DSA placement error. This is supported by the positive correlation coefficients between the two parameters above 0.5 for all data catergories.

## CONCLUSION

In conclusion, we have demonstrated the first measurements of placement accuracy for line-space patterns generated by chemoepitaxial diblock copolymer directed self-assembly in reference to the underlying chemical prepatterns. This measurement has been hampered previously by the fact that the chemical prepattern and resultant DSA-generated pattern are imaged separately, with no precise spatial alignment between the images. We address these limitations by introducing a prepattern design with an *in situ* registration mark—a unique central feature (here a single pinning line) that produces a registered single feature in the resultant DSA pattern that is easily identified by pattern symmetry. From this single feature, all pinned DSA features can be matched to their proper pinning feature. The use of an inorganic prepattern allows prepattern recovery after DSA by full polymer removal, avoiding any uncertainties or problems introduced by imaging the prepatterns before DSA, and multimodal registration of the prepattern and DSA pattern images to an intermediate image with both features present enables precise placement error measurements. From these initial results, we are able to outline the prepattern line CDs that will likely minimize DSA placement error for high-volume manufacturing, and we show that DSA placement error is positively correlated with prepattern nonuniformity due to the self-healing behavior of DSA. For prepattern pitches with minimal nonuniformity that are commensurate with a multiple of the block copolymer natural period, we anticipate DSA placement errors less than ~2 nm on a 25 nm pitch will be the norm.

The concept of *in situ* registration marks is a powerful tool for assessing the accuracy of chemoepitaxial registration, as it avoids added steps in sample preparation, minimizes the likelihood of perturbing the DSA process, and may be adapted to other chemoepitaxy process flows than the one described here. Further work will be necessary to understand the effect of other factors such as pitch commensurability or to extend the measurement to other types of chemical prepatterns. However, the encouraging results presented in this work suggest that DSA pattern placement error will compare favorably with factors such as overlay error, CD uniformity, and pattern edge roughness in lithographic steps required to delineate device features in the self-assembled patterns.

## EXPERIMENTAL SECTION

**Materials.** The poly(styrene-r-epoxydicyclopentadiene methacrylate) neutralization material was synthesized by traditional free-radical polymerization in methyl ethyl ketone using 2,2′-azobis(2-methylpropionitrile) initiator. Styrene:epoxydicyclopentadiene methacrylate feed ratio = 75:25, $M_n$ = 6.8 kg mol$^{-1}$, PDI = 1.50. The styrene:epoxydicyclopentadiene methacrylate molar ratio is approximately 74:26 by inverse-gated $^{13}$C NMR on neutralization material prepared in the same way but with lower molecular weight. For casting on a substrate the neutralization material was combined in solution with *N*-(trifluoromethylsulfonoxy) phthalimide thermal acid generator (10 wt % relative to polymer) in propylene glycol methyl ether acetate (PGMEA). Lamellae forming PS-PMMA ($M_n$ = 22 kg mol$^{-1}$ − 22 kg mol$^{-1}$; PDI = 1.09; estimated PMMA volume fraction = 0.51) was purchased from Polymer Source and used as received.

**Sample Preparation.** Si wafers were spin-coated with an 8 nm thick neutralization layer that was cross-linked by baking at 220 °C for 5 min in air. HSQ resist was spin-coated on top of this neutral layer. Subsequent exposure by electron beam lithography and development using standard developer solutions resulted in lines 2−5 nm in height in the patterns used for placement accuracy measurement described in the main text. PS-PMMA layers 37 or 48 nm thick were then spin-coated from 2% (w/w) in PGMEA and baked at 255 °C for 5 min in air. PMMA and PS were etched to various extents by oxygen reactive ion etching (approximately 2:1 etch rate ratio) for various times. The natural period of the PS-PMMA lamellae was determined by Fourier transform analysis of SEM images of fingerprint patterns occurring naturally over the neutral surface away from prepattern areas on the samples.

**Imaging and Analysis.** For the four data categories (3× or 4× frequency multiplication with 37 or 48 nm thick PS-PMMA films), nine sets of images corresonding to individual HSQ prepatterns were analyzed per category, except for 4× multiplication using 48 nm thick films in which six image sets were analyzed. In total, 54 to 107 single pinning line data points were collected per category. SEM images 768 × 1024 pixels in size at a resolution of 0.88 nm/pixel were obtained using a Leo 1550 field-emission SEM at a working distance of 3.0 mm. All image processing was performed using ImageJ unless noted otherwise. Background suppression and smoothing were accomplished simultaneously using a bandpass filter. Image contrast was enhanced by normalizing the range of pixel intensities to the maximum intensity range. Prepattern images and DSA images were both registered to the image of the same pattern at an intermediate etch step before full polymer removal using the MATLAB multimodal image registration function (translational and rotational transformations only) to put both images in the same reference frame. After image registration, DSA pattern images were thresholded at 50% of the maximum range. Prepattern images were thresholded similarly, but the threshold was inverted. Analysis was restricted to parallel line regions delineated by a bounding rectangle.

Line CD (width) values were defined as the area of each line divided by its height. Prepattern line centroid *x*-coordinates were fitted from left to right in the image to a line by least-squares fitting with an arbitrary origin, where the fitted slope reflects the nominal prepattern pitch. Prepattern placement error is defined as the difference between the measured line centroid *x*-coordinate and its best-fit position, equivalent to the residuals of the fit.

Centroid measurements are unbiased position estimates and are independent of the threshold value. Taking each line as a rectangle, the variance ($\sigma_x^2$) in centroid $x$-coordinate measurements in this work is estimated following the analysis of Ho:[26]

$$\sigma_x^2 \approx \frac{HW^2}{24A^2} \quad (3)$$

where $H$ and $W$ are the height and width of a bounding rectangle around the line, and $A$ is the line area. The use of a bounding rectangle to determine $H$ and $W$ sets them at maximum values of height and width for the line, respectively. Hence the obtained variance values are an overestimate. Nevertheless, the uncertainty in individual DSA placement error measurements based on the standard deviation of exact centroid positions of pinning lines and corresponding DSA spaces is less than 0.04 nm at the image resolution stated above. Thus, image resolution is not a limiting factor in DSA placement error measurement accuracy for this work.

Another possible source of error is misorientation between the prepattern and DSA pattern images. For nonzero rotational misorientation, variation in the positions of $y$-coordinates for feature centroids induces variation in the measured position of centroid $x$-coordinates for the same features. For a misorientation angle $\theta_{mis}$ (in radians) and a standard deviation in centroid $y$-coordinates $\sigma_y$, the uncertainty in centroid $x$-coordinate measurements is approximately $\sigma_y\theta_{mis}$. Both images are manually aligned so that straight lines are nearly parallel with the vertical image axis, and the misorientation angle is further minimized by the image registration process. From lines fitted to the straight portions of registered prepattern and DSA pattern images using a MATLAB-derived script, we obtained the average angles of these straight lines with the vertical image axis; the difference between these angles for corresponding registered prepattern and DSA pattern images provides a measure of the rotational misorientation. We found an average magnitude for $\theta_{mis}$ of $0.08 \pm 0.06°$. The standard deviation in measured centroid $y$-coordinates is negligible in DSA pattern images, but ranges between 30 and 90 nm in prepattern images due to roughness and discontinuities in the HSQ lines. Typical uncertainty in centroid $x$-coordinates arising from rotational misorientation between images is therefore less than 0.1 nm. Combining uncertainty due to centroid determination and image misorientation, we estimate a $3\sigma$ uncertainty in single DSA placement error measurements that is less than 0.3 nm.

The uncertainty induced by the translational misregistration of the prepattern and DSA images to an intermediate image is less clear. However, this uncertainty does not affect the DSA placement error $3\sigma$ values, and uncertainty for the mean DSA placement error values is based on the standard error of the mean.

**Free Energy Calculations.** The free energy per polymer chain ($F$) was computed by extending a standard model for lamellar block copolymers based on chain stretching and PS-PMMA interfacial tension contributions[27] to include a term reflecting the PS-HSQ interfacial tension:

$$\frac{F}{k_BT} = \frac{3(l/2)^2}{2Na^2} + \frac{\gamma_{PS\text{-}PMMA}}{k_BT}\Sigma + \frac{\gamma_{PS\text{-}HSQ}}{k_BT}\Theta \quad (4)$$

where $l$ is the total extent of the block copolymers passing through the interface in nm, $N$ is the degree of polymerization of the polymer, $a$ is the linear size of a monomer in nm, $\gamma_{PS\text{-}PMMA}$ the interfacial tension of the PS-PMMA interface, $\Sigma$ is the corresponding interfacial area per chain, $\gamma_{PS\text{-}HSQ}$ is the interfacial tension of the PS-HSQ interface, and $\Theta$ is the PS-HSQ area per chain. This model is approximate and does not apply for nonlamellar canonical or noncanonical block copolymer morphologies, for which more sophisticated models such as self-consistent field theory[28] would be required. For the present calculations, $a$ was set to 0.5 nm, $N$ was set to 800 monomer units, and both $\gamma_{PS\text{-}PMMA}$ and $\gamma_{PS\text{-}HSQ}$ were set to $0.28(k_BT)/\text{nm}^2$ based on observed experimental values for $\chi_{PS\text{-}PMMA}$.[29,30] Increasing the $\gamma_{PS\text{-}HSQ}$ to reflect strong PMMA-HSQ pinning would increase the stability of aligned *versus* misaligned lamellae, but does not change the value of $w$, in which rms placement error is minimized. For the model where interfaces are allowed to tilt, increasing $\gamma_{PS\text{-}HSQ}$ would increase the maximum degree of interfacial tilting observed. This choice of parameters yields a lamellar period $L_o$ of 24.7 nm. The total film thickness, needed to compute $\Theta$, was taken to be $3L_o/2$.

The simple model above was used to calculate the free energy of a system consisting of a central mobile PMMA domain (and associated two flanking PS half-domains for a total width of $L_o$) above a HSQ pinning line of width $w$. The central domain was flanked on either side by unpinned domains of total length $3L_o$. Each unpinned domain was assumed to be bounded on the outside by an immobile pinned domain, which was not included in the calculation. Displacement of the central mobile domain by a distance $\Delta$ changes the area of PS-HSQ contact $\Theta$ and expands one flanking domain by $+\Delta$ while compressing the other by $-\Delta$. For a particular pinning stripe width $w$, the expected root-mean-squared displacement $\langle\Delta^2\rangle^{1/2}$ was calculated by computing the free energy as a function of $\Delta$ for all displacements from $-L_o/2$ to $+L_o/2$ in increments of $0.01L_o/2$. The root-mean-squared displacement was then calculated as the partition function sum using these free energies:

$$\sqrt{\langle\Delta^2\rangle} = \left(\frac{\Sigma\Delta_i^{\,2}e^{-F(\Delta_i)/k_BT}}{\Sigma e^{-F(\Delta_i)/k_BT}}\right)^{1/2} \quad (5)$$

The simple model was further extended to take into account the possibility that the PS-PMMA interfaces of the mobile PMMA domain do not project normal from the substrate but instead tilt by an angle $\theta$ that is uniform throughout the film thickness. The total width of the mobile domain was treated as fixed at $0.5L_o$, so the tilted interface causes chain stretching and compression and increases the PS-PMMA interfacial area, but may decrease the area of unfavorable PS-HSQ interface. For this "tilt" model, each of the two PS-PMMA interfaces of the mobile PMMA domain were allowed to tilt independently. In effect, each PMMA domain was allowed to adopt a trapezoidal geometry if doing so minimized its free energy. More complex geometries where the deformation or tilt angle varied through the film thickness were not considered. The free energy per chain associated with each interface was computed for all possible $\theta$ from $-45$ to 45 degrees in increments of 0.1 degree. The $\theta$ minimizing the free energy was taken to be the tilt (and corresponding free energy) of that interface. A schematic of the tilted domain geometry and a plot of $\theta$ *versus* $w$ are included as Supporting Information. As above, the total free energy per chain of the system was calculated as a function of $\Delta$, taking tilting deformations into account, and used to compute the expected root-mean-squared displacement $(\langle\Delta^2\rangle_{tilt})^{1/2}$.

*Conflict of Interest:* The authors declare no competing financial interest.

*Acknowledgment.* This work is sponsored in part by the DARPA GRATE (Gratings of Regular Arrays and Trim Exposures) program under Air Force Research Laboratory (AFRL) contract FA8650-10-C-7038. The views expressed are those of the author and do not reflect the official policy or position of the Department of Defense or the U.S. Government. Approved for public release; distribution is unlimited.

*Supporting Information Available:* A schematic of the tilted domain geometry and a plot of $\theta$ *versus* $w$. This material is available free of charge *via* the Internet at http://pubs.acs.org.

‡Present address: IBM Albany Nanotech, 257 Fuller Road, Albany, New York 12203, United States.

## REFERENCES AND NOTES

1. Arnold, W. Double Patterning Lithography. *J. Micro/Nanolith. MEMS, MOEMS* **2009**, *8*, 011001.
2. Segalman, R.; Yokoyama, H.; Kramer, E. Graphoepitaxy of Spherical Domain Block Copolymer Films. *Adv. Mater.* **2001**, *13*, 1152–1155.
3. Jung, Y.; Ross, C. Orientation-Controlled Self-Assembled Nanolithography Using a Polystyrene-Polydimethylsiloxane Block Copolymer. *Nano Lett.* **2007**, *7*, 2046–2050.

4. Jeong, S.; Kim, J.; Moon, H.; Kim, B.; Kim, S.; Kim, J.; Kim, S. Soft Graphoepitaxy of Block Copolymer Assembly with Disposable Photoresist Confinement. *Nano Lett.* **2009**, *9*, 2300–2305.
5. Chai, J.; Wang, D.; Fan, X.; Buriak, J. Assembly of Aligned Linear Metallic Patterns on Silicon. *Nat. Nanotechnol.* **2007**, *2*, 500–506.
6. Yang, J.; Jung, Y.; Chang, J.; Mickiewicz, R.; Alexander-Katz, A.; Ross, C.; Berggren, K. Complex Self-Assembled Patterns Using Sparse Commensurate Templates with Locally Varying Motifs. *Nat. Nanotechnol.* **2010**, *5*, 256–260.
7. Cheng, J.; Sanders, D.; Truong, H.; Harrer, S.; Friz, A.; Holmes, S.; Colburn, M.; Hinsberg, W. Simple and Versatile Methods to Integrate Directed Self-Assembly with Optical Lithography Using a Polarity-Switched Photoresist. *ACS Nano* **2010**, *4*, 4815–4823.
8. Yi, H.; Bao, X.; Zhang, J.; Bencher, C.; Chang, L.; Chen, X.; Tiberio, R.; Conway, J.; Dai, H.; Chen, Y.; *et al.* Flexible Control of Block Copolymer Directed Self-Assembly Using Small, Topographical Templates: Potential Lithography Solution for Integrated Circuit Contact Hole Patterning. *Adv. Mater.* **2012**, 10.1002/adma.201200265.
9. Kim, S.; Solak, H.; Stoykovich, M.; Ferrier, N.; de Pablo, J.; Nealey, P. Epitaxial Self-Assembly of Block Copolymers on Lithographically Defined Nanopatterned Substrates. *Nature* **2003**, *424*, 411–414.
10. Stoykovich, M.; Muller, M.; Kim, S.; Solak, H.; Edwards, E.; de Pablo, J.; Nealey, P. Directed Assembly of Block Copolymer Blends into Nonregular Device-Oriented Structures. *Science* **2005**, *308*, 1442–1446.
11. Ruiz, R.; Kang, H.; Detcheverry, F.; Dobisz, E.; Kercher, D.; Albrecht, T.; de Pablo, J.; Nealey, P. Density Multiplication and Improved Lithography by Directed Block Copolymer Assembly. *Science* **2008**, *321*, 936–939.
12. Cheng, J.; Rettner, C.; Sanders, D.; Kim, H.; Hinsberg, W. Dense Self-Assembly on Sparse Chemical Patterns: Rectifying and Multiplying Lithographic Patterns Using Block Copolymers. *Adv. Mater.* **2008**, *20*, 3155–3158.
13. Liu, C.; Nealey, P.; Raub, A.; Hakeem, P.; Brueck, S.; Han, E.; Gopalan, P. Integration of Block Copolymer Directed Assembly with 193 Immersion Lithography. *J. Vac. Sci. Technol. B* **2010**, *28*, C6B30–C6B34.
14. Stoykovich, M.; Daoulas, K.; Muller, M.; Kang, H.; de Pablo, J.; Nealey, P. Remediation of Line Edge Roughness in Chemical Nanopatterns by the Directed Assembly of Overlying Block Copolymer Films. *Macromolecules* **2010**, *43*, 2334–2342.
15. Bencher, C.; Smith, J.; Miao, L.; Cai, C.; Chen, Y.; Cheng, J.; Sanders, D.; Tjio, M.; Truong, H.; Holmes, S.; *et al.* Self-Assembly Patterning for Sub-15nm Half-Pitch: A Transition from Lab to Fab. *Proc. SPIE* **2011**, *7970*, 79700F.
16. Bencher, C.; Yi, H.; Zhou, J.; Cai, M.; Smith, J.; Miao, L.; Montal, O.; Blitshtein, S.; Lavia, A.; Dotan, K.; *et al.* Directed Self-Assembly Defectivity Assessment (Part II). *Proc. SPIE* **2012**, *8323*, 83230N.
17. Liu, C.; Thode, C.; Delgadillo, P. R.; Craig, G.; Nealey, P. Towards an All-Track 300 mm Process for Directed Self-Assembly. *J. Vac. Sci. Technol. B* **2011**, *29*, 06F203.
18. Ruiz, R.; Dobisz, E.; Albrecht, T. Rectangular Patterns Using Block Copolymer Directed Assembly for High Bit Aspect Ratio Patterned Media. *ACS Nano* **2011**, *5*, 79–84.
19. Liu, C.; Craig, G.; Kang, H.; Ruiz, R.; Nealey, P. Practical Implementation of Order Parameter Calculation for Directed Assembly of Block Copolymer Thin Films. *J. Polym. Sci., Part B: Polym. Phys.* **2010**, *48*, 2589–2603.
20. Gido, S.; Thomas, E. Lamellar Diblock Copolymer Grain Boundary Morphology. 4. Tilt Boundaries. *Macromolecules* **1994**, *27*, 6137–6144.
21. Liu, C.; Han, E.; Onses, M.; Thode, C.; Ji, S.; Gopalan, P.; Nealey, P. Fabrication of Lithographically Defined Chemically Patterned Polymer Brushes and Mats. *Macromolecules* **2010**, *44*, 1876–1885.
22. Edwards, E.; Muller, M.; Stoykovich, M.; Solak, H.; de Pablo, J.; Nealey, P. Dimensions and Shapes of Block Copolymer Domains Assembled on Lithographically Defined Chemically Patterned Substrates. *Macromolecules* **2007**, *40*, 90–96.
23. Stein, G.; Liddle, J.; Aquila, A.; Gullikson, E. Measuring the Structure of Epitaxially Assembled Block Copolymer Domains with Soft X-Ray Diffraction. *Macromolecules* **2010**, *43*, 433–441.
24. Felix, N.; Gabor, A.; Menon, V.; Longo, P.; Halle, S.; Koay, C.; Colburn, M. Overlay Improvement Roadmap: Strategies for Scanner Control and Product Disposition for 5 nm Overlay. *Proc. SPIE* **2012**, *7971*, 79711D.
25. Laidler, D.; D'have, K.; Hermans, J.; Cheng, S. Mix and Match Overlay Optimization Strategy for Advanced Lithography Tools (193i and EUV). *Proc. SPIE* **2011**, *8326*, 83260M.
26. Ho, C. Precision of Digital Vision Systems. *IEEE Trans. Pattern Anal. Mach. Intell.* **1983**, *5*, 593–601.
27. Bates, F. S.; Fredrickson, G. H. Block Copolymers—Designer Soft Materials. *Phys. Today* **1999**, *52*, 32–38.
28. Fredrickson, G. H. *The Equilibrium Theory of Inhomogeneous Polymers*; Oxford University Press: New York, USA, 2006.
29. Ahn, H.; Ryu, D. Y.; Kim, Y.; Kwon, K. W.; Lee, J.; Cho, J. Phase Behavior of Polystyrene-b-Poly(Methyl Methacrylate) Diblock Copolymer. *Macromolecules* **2009**, *42*, 7897–7902.
30. Zhao, Y.; Sivaniah, E.; Hashimoto, T. SAXS Analysis of the Order-Disorder Transition and the Interaction Parameter of Polystyrene-block-Poly(Methyl Methacrylate). *Macromolecules* **2008**, *41*, 9948–9951.